

Capturing Anatomical Shape Variability Using B-spline Registration

Thomas H. Wenckeback, Hans Lamecker, and Hans-Christian Hege

Zuse Institute Berlin (ZIB),
Takustr. 7, 14195 Berlin, Germany,
{wenckeback,lamecker,hege}@zib.de, www.zib.de/visual

Abstract. Registration based on B-spline transformations has attracted much attention in medical image processing recently. Non-rigid registration provides the basis for many important techniques, such as statistical shape modeling. Validating the results, however, remains difficult - especially in intersubject registration. This work explores the ability of B-spline registration methods to capture intersubject shape deformations. We study the effect of different established and new shape representations, similarity measures and optimization strategies on the matching quality. To this end we conduct experiments on synthetic shapes representing deformations which typically may arise in intersubject registration, as well as on real patient data of the liver and pelvic bone. The experiments clearly reveal the influence of each component on the registration performance. The results may serve as a guideline for assessing intensity based registration.

1 Introduction

Motivation. Detailed analysis of anatomical shape variability frequently depends on identification of corresponding points on different shapes. Morphological studies, like neuroanatomical studies of the brain, generation of anatomical atlases, and many other applications demand such information. In recent times statistical shape modeling has been proven a successful method in medical image processing. The performance of statistical shape models crucially depends on the way anatomical regions of different shapes are mapped to each other. Anatomical correspondence across different subjects is not well understood, and hence much harder to validate than in intrasubject matching.

Volumetric registration of medical data using B-spline transformations has been widely applied in medical image processing [1–5]. In many cases registration is performed directly on (tomographic) image data which implicitly contains the shape of the object. In this work we will explore the capability of B-spline based registration methods to capture shape variability. Therefore we focus on registration of surfaces, where the deformation model itself can be studied more accurately without interference originating from image-related mismatches. Particularly in intersubject registration large deformations may occur. Anatomically corresponding structures may differ geometrically or may be separated widely, see for instance Fig. 1.



Fig. 1. Comparison of different liver registrations with equal surface distance: *Left:* Template. *Mid:* Triangulation registration with boundary constraints (similar result for distance field registration), *Right:* Triangulation registration without boundary constraints (similar result for label field) leads to incorrect anatomical matching

Contributions. The aim of this work is to study the influence of different shape representations, similarity measures as well as optimization strategies on the performance of the B-spline based registration framework. To this end we define a set of pairs of synthetic shapes that represent deformations which typically may arise in intersubject registration. Moreover, we consider two anatomical shapes of different variability: liver consists of soft tissue, and its shape is subject to respiratory state, patient pose, and configuration of neighbouring organs, while pelvic bone is basically a rigid structure. Here, additional anatomical expert knowledge is available for validation. We evaluate the performance measured in terms of surface distance after registration, regularity of the deformation map, robustness and landmark placement. These experiments clearly reveal strengths and weaknesses of the different components under investigation.

Previous Work. Fleute et al. [6] first used intersubject non-rigid registration for building a statistical shape model of the knee. They employed the algorithm by Szeliski and Lavallée [1] using asymmetric surface distance as similarity measure. Frangi et al. applied Rückert’s registration [2] based on label fields for CT bone, MRI brain data [7], and cardiac images [8]. They compare their method to the work of Brett et al. [9], who use a symmetric variant of the rigid iterative closest-points algorithm (ICP) [10] for brain data. Non-rigid extensions to ICP have been reported recently [11, 12]. Rohlfing et al. [3] employed the algorithm by Rückert for construction of an anatomical atlas of the honey bee.

The capability of the deformation model has not been analyzed thoroughly up to now. It was assumed that correspondences based on B-spline registration are fold-over free [7] as opposed to those obtained by the ICP approach of Brett et al. We show this to be generally not the case. Usually, validation is performed indirectly by assessing the performance of the derived shape models or in terms of the implemented similarity measures. Rohlfing et al. evaluate the quality (sharpness, entropy) of the averaged intensity image obtained by their registration. Frangi et al. [8] consider landmark correspondence.

Instead of surfaces, lower dimensional structures such as landmarks [13] or feature curves [14] are in use. Unfortunately, for many organs like the liver such descriptions are difficult to derive due to a lack of characteristic shape features.

Incorporation of geometric features into ICP can be found in [15, 16]. Wang et al. [17] base their semi-automatic matching on curvature classifiers. A fundamentally different approach to non-rigid matching is based on mappings of two-dimensional manifolds [18–20], as opposed to volumetric mappings.

2 Algorithmic Overview

The task of volumetric registration is to find a spatial mapping $\mathbf{T} : \mathbb{R}^3 \rightarrow \mathbb{R}^3$ between a *template* shape X and a *target* shape Y , such that X and Y resemble each other as much as possible. The similarity of X and Y is defined by some cost function $E(\mathbf{T}, X, Y)$. We will study the following shape representations:

Label fields (LF) $A : \Omega_A \rightarrow \mathcal{L}_A$ with $\mathcal{L}_A \subset \mathbb{Z}$ implicitly contain the boundary along voxels belonging to different segments \mathcal{L}_A ($= \{0, 1\}$ for binary images). Label fields with smooth boundaries are generated by scan-conversion of triangulated surfaces.

Signed distance fields (SDF) $A : \Omega_A \rightarrow \mathcal{D}_A$ with $\mathcal{D}_A \subset \mathbb{R}$ encoding for each voxel the spatial distance to the closest point of a surface. It’s level sets implicitly represent a family of shapes. A is computed via euclidean distance mapping [21].

Triangulated surfaces (TS) $\mathcal{S}_A \subset \mathbb{R}^3$ are the only parametric shape representations considered in this work. Triangulated surfaces are typically generated by segmentations of tomographic data using the marching cubes algorithm.

In the framework of parametric registration, the transformation \mathbf{T} is composed of an affine transformation $\mathbf{T}_{\text{affine}}$ as well as a B-spline deformation $\mathbf{T}_{\text{B-spline}}$. The latter is defined on a 3D discrete uniform control point grid (CPG) with cubic B-spline interpolation between adjacent control points, see [2, 4] for details. The B-spline deformation model appears suitable for intersubject registration, because it provides smooth deformations when a physical model is not known.

The optimal transformation \mathbf{T} for a given cost function E is determined by a nonlinear multilevel optimization scheme. The CPG is refined iteratively, providing a parameter pyramid, while at the same time there is a data pyramid consisting of several sampled versions of the shapes. The main intention of this approach is to prevent optimization from being trapped in a local minimum of the similarity criterion. By means of B-spline CPG refinement global deformations are corrected at the beginning, while local deformations are iteratively resolved later on. The minimum \mathbf{T}^* of the cost function E is found by employing a gradient descent-like search strategy. Instead of numerically approximating the gradient, a *search-direction* is computed by scanning the whole parameter space within some capture range depending on the level within the data pyramid [22].

The general cost function of the registration consists of a term measuring shape similarity D , a regularization term R smoothing the transformation, plus additional boundary constraints:

$$E(\mathbf{T}, X, Y) = D(\mathbf{T}(X), Y) + \lambda R(\mathbf{T}) + \text{boundary constraints} , \quad (1)$$

where the shape similarity D consists of a weighted sum of different measures:

Similarity Measure 1 (Label Consistency). Given label fields A, B , with labels $\mathcal{L} = \{1, \dots, L\}$ and image domain Ω , let $p_{AB}(l, m)$ denote the probability of



Fig. 2. Problem of asymmetric distance measures. *Left:* Initial template and target. *Mid:* Result with one-sided surface distance. *Right:* Schematic view

cooccurrence of labels $l, m \in \mathcal{L}$ in the overlap domain $\Omega_{A,B}$. Label consistency [8] is measured by

$$D_{\mathcal{L}}(A, B) = \sum_{l=1}^L p_{AB}(l, l). \quad (2)$$

Similarity Measure 2 (Grey-Value Difference). For distance fields A and B , grey-value difference is defined as

$$D_{\mathcal{D}}(A, B) = \frac{1}{|\Omega_{A,B}|} \sum_{\mathbf{x} \in \Omega_{A,B}} [A(\mathbf{x}) - B(\mathbf{x})]^2. \quad (3)$$

For triangulations \mathcal{S}_A and \mathcal{S}_B let $d_s(\mathbf{p}, \mathcal{S}_B) = \min_{\mathbf{q} \in \mathcal{S}_B} \|\mathbf{p} - \mathbf{q}\|_2$ denote the distance of a point \mathbf{p} on \mathcal{S}_A to the surface \mathcal{S}_B . Based on d_s , we define the closest point \mathbf{c} on \mathcal{S}_B to \mathbf{p} on \mathcal{S}_A by $\mathbf{c}(\mathbf{p}, \mathcal{S}_B) = \arg \min_{\mathbf{q} \in \mathcal{S}_B} \|\mathbf{p} - \mathbf{q}\|_2$. Obviously, this correspondence is asymmetric (cf. Fig. 2, right). We propose to use a symmetric surface distance as the fundamental similarity measure for shapes:

Similarity Measure 3 (Surface Distance) is defined by

$$D_s(\mathcal{S}_A, \mathcal{S}_B) = \frac{1}{|\mathcal{S}_A| + |\mathcal{S}_B|} \left(\sqrt{\sum_{\mathbf{p} \in \mathcal{S}_A} d_s(\mathbf{p}, \mathcal{S}_B)^2} + \sqrt{\sum_{\mathbf{q} \in \mathcal{S}_B} d_s(\mathbf{q}, \mathcal{S}_A)^2} \right). \quad (4)$$

Note that measures employed on triangulations should be symmetric in order to match convex or concave regions as illustrated in Fig. 2, left. This implies a considerable algorithmic complexity in contrast to the conventional asymmetric scheme: the latter can be implemented efficiently using a distance map of the target surface, while the former requires at any partial derivative calculation a search for closest points.

Local geometric characterizations of surfaces are often included in the cost function to improve the matching. Particularly in intersubject registration, situations are common where anatomical structures are pronounced to a highly different degree, yet spatially aligned closely (cf. Fig. 3). Such problems may be avoided by incorporating the normal vector fields \mathbf{n}_A and \mathbf{n}_B of the surfaces:

Similarity Measure 4 (Normal Deviation) is defined by

$$D_n(\mathcal{S}_A, \mathcal{S}_B) = \frac{1}{|\mathcal{S}_A| + |\mathcal{S}_B|} \left(\sum_{\mathbf{p} \in \mathcal{S}_A} d_n(\mathbf{p}, \mathcal{S}_B)^2 + \sum_{\mathbf{q} \in \mathcal{S}_B} d_n(\mathbf{q}, \mathcal{S}_A)^2 \right), \quad (5)$$

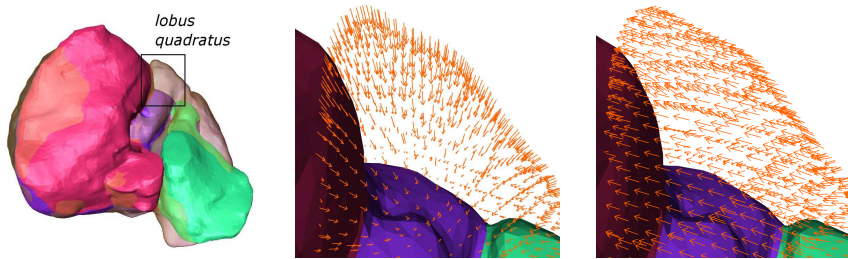


Fig. 3. Ambiguity induced by a spatial attractor. The anatomically corresponding region in the middle (l. quadr.) is hardly pronounced on the target. *Left:* Overview. *Mid:* Close-up: displacements for correct solution. *Right:* Displacements for bad solution.

with $d_n(\mathbf{p}, \mathcal{S}_B) = 1 - \mathbf{n}_A(\mathbf{p}) \cdot \mathbf{n}_B(\mathbf{c}(\mathbf{p}, \mathcal{S}_B))$.

Other commonly used local geometric characterizations are based on the principal curvatures κ_1 and κ_2 of a surface. Koenderink and van Doorn [23] introduced two suitable classifiers: the so-called shape index $S = \frac{2}{\pi} \arctan \frac{\kappa_1 + \kappa_2}{\kappa_2 - \kappa_1}$ with $\kappa_2 \neq \kappa_1$ separates a surface into convex, hyperbolic and concave areas, and transitions between these; the range is continuous within $[-1, 1]$. Note that S is invariant under global scaling of the surface. The curvedness $C = \sqrt{\frac{\kappa_1^2 + \kappa_2^2}{2}}$ is a suitable classifier when scale is of interest. It also has some advantages over the mean curvature: the mean curvature vanishes at points where $\kappa_1 = -\kappa_2$ and its magnitude is not intuitive, since it does not grow proportionally with the radius of a sphere. Both defects are cured by the curvedness C . Misregistrations as shown in Fig. 4 can be avoided by using such information.

Similarity Measure 5 (Curvature Similarity). Let curv denote either the shape index S or the curvedness C . Curvature similarity is defined as

$$D_{\text{curv}}(\mathcal{S}_A, \mathcal{S}_B) = \frac{1}{|\mathcal{S}_A| + |\mathcal{S}_B|} \left(\sum_{\mathbf{p} \in \mathcal{S}_A} d_c(\mathbf{p}, \mathcal{S}_B)^2 + \sum_{\mathbf{q} \in \mathcal{S}_B} d_c(\mathbf{q}, \mathcal{S}_A)^2 \right), \quad (6)$$

with $d_c(\mathbf{p}, \mathcal{S}_B) = \text{curv}(\mathbf{p}) - \text{curv}(\mathbf{c}(\mathbf{p}, \mathcal{S}_B))$.

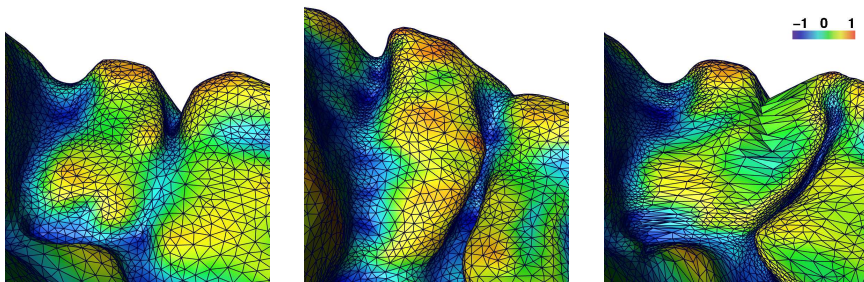


Fig. 4. Plain LF registration. *Left:* Target. *Mid:* Template. *Right:* Misregistration (shape index colouring of original template is transferred to deformed template)

Regularization (Grid Energy). Large deformations in intersubject registration, as well as over-refinement of the CPG may lead to irregular B-spline deformations. Therefore, in some applications we use a regularization term R in the cost function, which models the bending energy of a thin metal plate (biharmonic model, see [1, 2]).

Boundary Constraint (Landmarks). We encountered situations in intersubject registration where all of the above similarity measures with or without regularization fail to achieve a reasonable registration. In this case, boundary constraints expressed by the sum of squared differences of manually specified corresponding landmarks on the template and the target shape may guide the optimization towards a better solution. In practice, reliable placement of landmarks on organs like the liver is possible in rare cases, only.

3 Results

Implementation. All components of the algorithm are implemented in one software framework in optimized C++ code. Increased performance is achieved by exploiting separability of B-spline interpolation and incremental evaluation of similarity measures. Adaptive CPG refinement is accomplished by switching off control points away from the template surface (for TS and LF registration only).

As a benchmark for evaluating the matching capability of the B-spline registration framework we identify three classes of deformations typically arising in intersubject registration:

Large deformations occur when corresponding structures lie spatially far apart, even after affine registration. As an example, consider Fig. 4: the concave structure (“valley”) should be coloured in blue after successful matching. Instead, it is mapped to the convex region to the right. The “cigar”/“banana” pair in Fig. 5 exemplifies this problem.

Spatial attractors may cause ambiguities in the registration. In Fig. 3 the lobus quadratus of the template shape might be deformed towards the left (lobus dexter), or down towards the anatomically correct region, which is hard to detect on the target. This situation is represented by “two hills” shapes in Fig. 5.

Absent features on one shape, which exist on the other, inevitably introduce some degree of arbitrariness. In the liver, neighbouring organs or vessels often cause deformations to a very different degree (cf. Fig. 9). Such cases are accentuated in an extreme fashion by the “muffin” shapes in Fig. 5.

We consider the following criteria in our evaluation of registration performance: a necessary requirement for a correct matching is a value for surface distance D_s close to zero. Moreover, the transformation \mathbf{T} should be regular, i.e. the determinant of the Jacobian $|\mathbf{J}_T|$ must be positive for each CPG cell. Additionally, for synthetic shapes we examine the euclidean distance of manually defined target points (*target point deviation* d_t in percentage of the shape diameter).

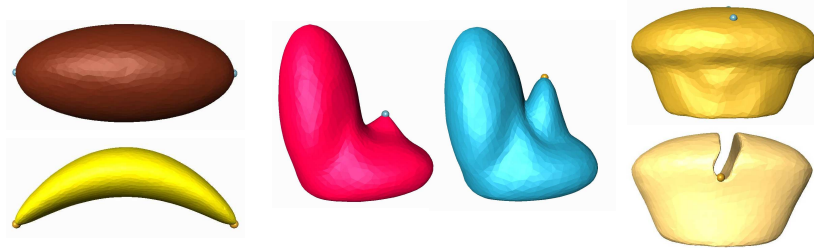


Fig. 5. Synthetic test shapes with target points (available for download at www.zib.de/wenckebach/ipmi05). *Left:* Problem 1: cigar/banana. *Mid:* Problem 2: two hills. *Right:* Problem 3: muffins

3.1 Experiments: Synthetic Shapes

The optimization starts on a coarse CPG ($5 \times 5 \times 5$), which is successively refined to $19 \times 19 \times 19$. The results of all experiments are sensitive to the initial CPG resolution. As a general rule, we found that matching quality improves when the resolution of the CPG is adapted to the frequency content of the shape.

The step width for the search direction is iteratively decreased from 10% of shape diameter on the initial to 0.05% on the final level. A higher initial CPG resolution was necessary for LF and SDF registration of the muffins. In all cases the surface distance vanishes after registration except for the muffin shapes using SDF or LF registration. Regularity is violated whenever using TS registration. Moreover, all experiments show that registration is *not* robust with respect to the weighting of the geometric similarity measures.

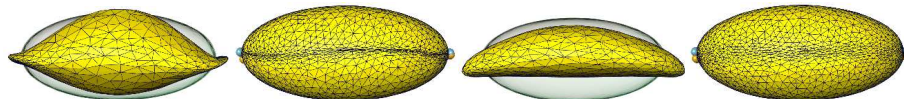


Fig. 6. Results banana. *Left:* TS registration with curvedness (1st level, result). *Right:* Combination of SDF and TS registration with curvedness (1st level, result)

Banana. For TS registration, the best result is shown in Fig. 6, left ($d_t = 3.3\%$). Carefully adjusting the weight of curvedness in the cost function improves matching the cusps. Yet, distortions are spread unevenly over the surface and there is little regularity. Amplifying the grid energy reduces surface distortion at the cost of larger target point deviation ($d_t = 8.3\%$). SDF registration combined with curvedness yields better results ($d_t = 2.8\%$), cf. Fig. 6 right. Neither shape index ($d_t = 47.8\%$) nor normal deviation ($d_t = 11.7\%$) lead to improvements.

Two Hills. Shape representation plays a crucial role in this example: SDF registration yields nearly perfect target point deviation of $d_t = 0.7\%$, whereas LF works satisfactorily only with a much larger initial search width ($d_t = 9.3\%$). TS registration leads to large mismatches with $d_t = 13.3\%$, which is improved

by using normal deviation ($d_t = 1\%$) or shape index ($d_t = 1.3\%$), cf. Fig. 7. Curvedness performs better ($d_t = 0.7\%$) at the cost of enormous surface distortions; grid energy alleviates this. Both shape index and curvedness produce irregular deformations.

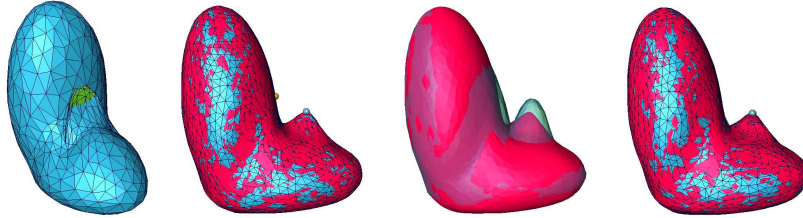


Fig. 7. Results two hills. *Left:* TS registration (1st level, result). *Right:* TS with normal deviation (1st level, result)

Muffin. Implicit representations require higher CPG resolution to accomplish a satisfactory target point deviation (LF: $d_t = 6.3\%$, SDF: $d_t = 7.9\%$). TS registration has larger target point deviation of $d_t = 8.4\%$, which is improved by considering normal deviation ($d_t = 5.8\%$); curvature measures yield no improvements. TS registration produces severe surface foldings, while SDF registration shows massive surface distortions (cf. Fig. 8). SDF registration will often fail in such cases, since deformations along the surface are ill-defined. Grid energy fails to alleviate this problem due to unacceptable matching quality.

The performance in terms of CPU time is – in all cases – best using LF or TS registration with one-sided surface distance. SDF representation is worse by a factor of 5, while symmetric TS registration increases the runtime by a factor of 20, due to the complexity of evaluating the two-sided surface distance.

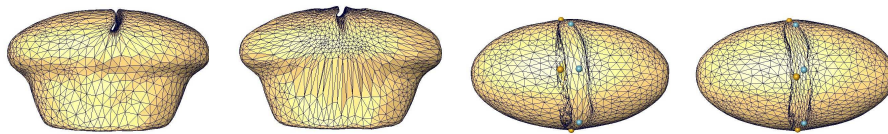


Fig. 8. Results muffin. *From left to right:* LF, SDF (surface distortion), TS registration (severe surface foldings), TS with normal deviation (improved matching)

3.2 Experiments: Anatomical Shapes

The optimization starts on a CPG of about 100 mm grid spacing, which is successively refined to 5 mm. For the LF representation an increased search width is employed. No geometric similarity measures are incorporated into the cost function, as this would require an extensive parameter study for the relative weights within the cost function.

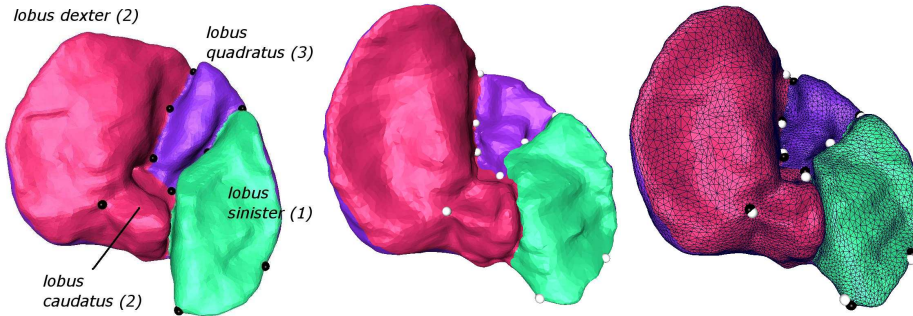


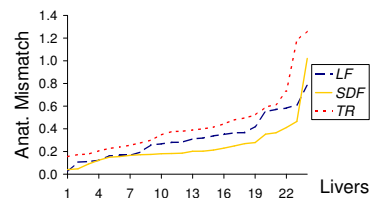
Fig. 9. SDF registration for the liver. Anatomically corresponding regions can be identified by their colour; target point locations indicate matching errors. *Left:* Template after affine registration. *Mid:* Target. *Right:* Resulting deformed template. The “valleys” of the template are not matched perfectly, yet the transformation remains regular; surface distortion is moderate, anatomical matching is satisfactory

Liver. The sample consists of 24 individuals. All shapes are registered to one target shape. Registration based on distance fields is always performed in combination with regularization to avoid distortions as present in the muffin example (cf. Fig. 8). The grid energy is applied adaptively on the last two levels of the optimization ($\lambda = 0.002/0.01$).

Anatomical mismatch is measured by the overlap d_o of corresponding anatomical regions (patches) of the liver. The surface distance is computed among corresponding patches only, and afterwards divided by D_s : the smaller d_o , the better the anatomical match. Although these regions cannot in general be specified uniquely, this measure is less sensitive to errors than individual landmark placement. The following regions were defined by medical experts (cf. Fig. 9): (1) lower left lobe, (2) lower right lobe plus caudate lobe, (3) lower quadratic lobe and (4) whole upper part of the liver. Cases of large anatomical mismatches (cf. Fig. 1) could be resolved by using landmark based boundary constraints. A typical result is shown in Fig. 9. Quantitative results are given in Tab. 1.

Table 1. Results for registration of real patient data (GE grid energy). Maximum and median of surface distance over the whole set, as well as the mean percentage of surface distance above a threshold of 2 mm is given. Average CPU times refer to a SGI system with 500 MHz MIPS R14k processor. For liver data, a histogram of anatomical mismatch (log. scale) is provided

| shape class | method | D_s [mm] | | > 2 [%] | CPUtime |
|-------------|--------|------------|------|-----------|------------|
| | | max | med | mean | [hh:mm:ss] |
| liver | LF | 0.71 | 0.49 | 4.73 | 00:42:45 |
| | SDF GE | 1.27 | 0.44 | 3.84 | 25:11:33 |
| | TS | 0.44 | 0.32 | 0.71 | 11:40:49 |
| pelvic bone | LF | 0.74 | 0.61 | 4.75 | 01:22:04 |
| | SDF | 0.83 | 0.45 | 1.98 | 03:10:09 |
| | TS | 0.38 | 0.34 | 0.33 | 31:35:24 |



Pelvic Bone. The sample comprises 17 male individuals. The target shape is reconstructed from the male visible human data set. One exemplary result is shown in Fig. 10. Quantitative results over the whole sample are given in Tab. 1. The deformation map is fold-over free for all shape representations. Visual inspection shows virtually no anatomical mismatch in all cases apart from the LF registrations, where the variability of the bending of the sacrum is not captured correctly (only 6 correct results).

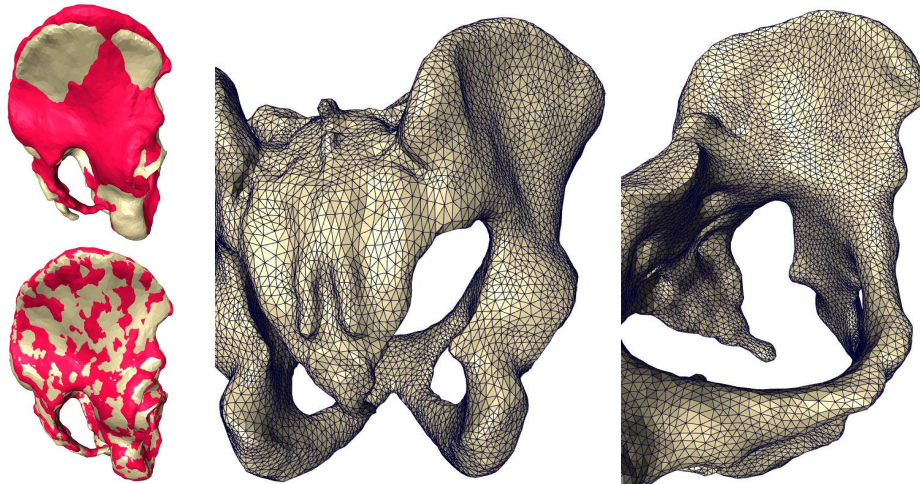


Fig. 10. SDF registration for pelvic bone. *Left:* Initial setting, result. *Mid, right:* Deformed template (with little surface distortion)

4 Discussion and Conclusion

We studied the ability of a registration framework based on B-spline transformations to capture intersubject shape variability. To this end we identified three different classes of typical deformations, which we represented by three different synthetic shapes. Moreover, two anatomical objects of different degrees of variability were examined. For our experiments we varied the essential components of the framework: shape representation, similarity measure and optimization strategy. The performance was measured in terms of surface distance between the deformed template and the target shape, regularity of the transformation \mathbf{T} , robustness and correspondence of landmark points or regions.

Optimization Strategies. The resolution of the CPG plays a crucial role. Although B-spline transformations are indeed capable of capturing large shape deviations, the control point spacing should be adapted to the frequency content of the shapes. This was shown by the banana/cigar example, where most of the deformation takes place around the cusps. Harmonic analysis of the shapes may

be a suitable pre-processing step for building adaptive control grids.

Similarity Measures. Using the symmetric surface distance is very costly, yet may be needed in cases where deformations are large. Weighting the terms in the cost function is a difficult task, especially between surface distance and geometric features. Although it seems fairly clear for the synthetic shapes, which geometric similarity is feasible to use, one cannot deduce from this the correct cost function for the anatomical examples. Completely different cost functions may certainly be more suitable for other applications. We found that the grid energy as a regularizer often is too restrictive to recover large deformations. To prevent large surface distortions, yet obtain good matchings, regularizers constraining deformation in the tangential directions of the shapes rather than in the normal direction should be employed.

Shape Representations. Of all shape representations used the SDF approach performed best. Triangulation based registration often lead to irregular transformations, while label field registration yielded deficient matchings, both in terms of target point deviation for the synthetic shapes and of anatomical correspondence for the medical examples. This can be explained by the fact that distance fields contain more information than triangulated surfaces or label fields: the latter encode a single 2-dimensional manifold while distance fields contain a continuous set of manifolds by extending the surface into \mathbb{R}^3 , which is beneficial in the optimization process.

Since the shape of anatomical structures is contained only implicitly in medical image data (e.g. MRI or CT), it is a-priori uncertain whether B-spline transformations represent the appropriate deformation model. The results of our experiments may serve as a guideline for assessing such intensity based registration tasks.

Future work will be directed towards combining SDF representations with different regularizers. Moreover, cost functions with different structures than the one used here should be explored. As a general rule, any a-priori anatomical knowledge available should be included to support intersubject registration.

Acknowledgements. We thank the developers of Amira [24], a software framework for advanced visual data analysis, that has been used for this work. Funding for T.H. Wenkebach and H. Lamecker has been provided by Deutsche Forschungsgemeinschaft (DFG) through the research center MATHEON.

References

1. Szeliski, R., Lavallée, S.: Matching 3-d anatomical surfaces with non-rigid deformations using octree-splines. *IJCV* **18(2)** (1996) 171–186
2. Rückert, D., Sonoda, L.I., Hayes, C., Hill, D.L.G., Leach, M.O., Hawkes, D.J.: Non-rigid registration using free-form deformations: Application to breast MR images. *IEEE Trans Med Imaging* **18(8)** (1999) 712-721

3. Rohlfing, T., Brandt, R., Maurer, C.R., Menzel, R.: Bee brains, B-splines and computational democracy: Generating an average shape atlas. Proc. IEEE Workshop on Mathematical Methods in Biomedical Image Analysis (2001) 187–194
4. Kybic, J., Unser, M.: Fast parametric elastic image registration. IEEE Trans Med Imaging **12(11)** (2003) 1427–1441
5. Kabus, S., Netsch, T., Fischer, B., Modersitzki, J.: B-spline registration of 3D images with Levenberg-Marquardt optimization. Proc. SPIE MI **5370** (2004) 304–313
6. Fleute, M., Lavallée, S., Julliard, R.: Incorporating a statistically based shape model into a system for computed-assisted anterior cruciate ligament surgery. MIA **3(3)** (1999) 209–222
7. Frangi, A.F., Rückert, D., Schnabel, J.A., Niessen, W.J.: Automatic 3D ASM construction via atlas-based landmarking and volumetric elastic registration. Proc. IPMI (2001) 78–79
8. Frangi, A.F., Rückert, D., Schnabel, J.A., Niessen, W.J.: Multiple-object three-dimensional shape models: Application to cardiac modeling. IEEE Trans Med Imaging **21(9)** (2002) 1151–1166
9. Brett, A.D., Taylor, C.J.: A method of automated landmark generation for automated 3D PDM construction. Imag Vis Comp **18(9)** (2000) 739–48
10. Besl, P.J., McKay, N.D.: A method for registration of 3-D shapes. IEEE Trans PAMI **14(2)** (1992) 239–256
11. Chui, H., Rangarajan, A.: A new point matching algorithm for non-rigid registration. CVIU **89(2–3)** (2003) 114–141
12. Xie, Z., Farin, G.: Image registration using hierarchical B-splines. IEEE Trans. on Visualization and Computer Graphics **10(1)** (2004) 85–94
13. Paulsen, R.R., Hilger, K.: Shape modelling using Markov random field restoration of point correspondences. Proc. IPMI (2003) 1–12
14. Subsol, G., Thirion, J.-P., Ayache, N.: A scheme for automatically building three-dimensional morphometric anatomical atlases: Application to skull atlas. MIA **2(1)** (1998) 37–60
15. Rusinkiewicz, S., Levoy, M.: Efficient variants of the ICP algorithm. Proc. of Third International Conference on 3D Digital Imaging and Modelling (2001) 145–152
16. Sharp, G.C., Lee, S.W., Wehe, D.K.: ICP registration using invariant features. IEEE Trans PAMI **24(1)** (2002) 90–102
17. Wang, Y., Peterson, B.S., Staib, L.H.: Shape-based 3D surface correspondence using geodesics and local geometry. Proc. CVPR (2000) 644–651
18. Kelemen, A., Székely, G., Gerig, G.: Three-dimensional model-based segmentation of brain MRI. IEEE Trans Med Imaging **18(10)** (1999) 828–839
19. Davies, R.H., Twining, C.J., Cootes, T.F., Waterton, J.C., Taylor, C.J.: 3D statistical shape models using direct optimisation of description length. Proc. 7th ECCV **3** (2002) 3–20
20. Lamecker, H., Lange, T., Seebaß, M.: A statistical shape model for the liver. Proc. MICCAI (2002) 422–427
21. Borgefors, G.: Distance transformations in digital images. Computer Vision, Graphics, and Image Processing **34** (1986) 344–371
22. Rohlfing, T.: Multimodale Datenfusion für die bildgesteuerte Neurochirurgie und Strahlentherapie. PhD thesis, Technische Universität Berlin (2000)
23. Koenderink, J.J., van Doorn, A.J.: Surface shape and curvature scales. IVC **10(8)** (1992) 557–565
24. Stalling, D., Westerhoff, M., Hege, H.-C.: Amira: A highly interactive system for visual data analysis. In: Hansen, C.D., Johnson C.R. (eds.): The Visualization Handbook (2005) 749–767